ADVANCED ENERGY MATERIALS
www.advenergymat.de

Highly Stable Supercapacitors with Conducting Polymer Core-Shell Electrodes for Energy Storage Applications

*Chuan Xia, Wei Chen, Xianbin Wang, Mohamed N. Hedhili, Nini Wei, and Husam N. Alshareef**

Conducting polymers such as polyaniline (PAni) show a great potential as pseudocapacitor materials for electrochemical energy storage applications. Yet, the cycling instability of PAni resulting from structural alteration is a major hurdle to its commercial application. Here, the development of nanostructured PAni–RuO_2 core–shell arrays as electrodes for highly stable pseudocapacitors with excellent energy storage performance is reported. A thin layer of RuO_2 grown by atomic layer deposition (ALD) on PAni nanofibers plays a crucial role in stabilizing the PAni pseudocapacitors and improving their energy density. The pseudocapacitors, which are based on optimized PAni–RuO_2 core–shell nanostructured electrodes, exhibit very high specific capacitance (710 F g^{-1} at 5 mV s^{-1}) and power density (42.2 kW kg^{-1}) at an energy density of 10 Wh kg^{-1}. Furthermore, they exhibit remarkable capacitance retention of ≈88% after 10 000 cycles at very high current density of 20 A g^{-1}, superior to that of pristine PAni-based pseudocapacitors. This prominently enhanced electrochemical stability successfully demonstrates the buffering effect of ALD coating on PAni, which provides a new approach for the preparation of metal-oxide/conducting polymer hybrid electrodes with excellent electrochemical performance.

1. Introduction

The intermittent nature of several sustainable energy sources such as solar and wind energy has ignited the demand of energy storage materials and devices.[1] Batteries are the most commonly used devices in energy storage systems. In spite of their affordability and large energy density, batteries suffer from serious shortcomings such as low power density and short cycling life.[2,3] In contrast, supercapacitors represent another important energy storage device, which can offer much longer life cycle and higher power density than batteries. Thus, supercapacitors are emerging as critical components to complement or even replace batteries in various applications. Therefore, the development of supercapacitors with higher energy and power outputs, and long cycling stability is urgently required.[3–9] According to the mechanism of energy storage, supercapacitors could be generally divided into two types: electrochemical double-layer capacitors (EDLCs) in which capacitance arises from charge accumulation in the electrode/electrolyte interface, and pseudocapacitors that are based on the fast and reversible redox reactions at the surface of electro-active materials.[3,5,10] Hence, in general, the capacitance of pseudocapacitors is much higher than EDLCs. Carbonaceous materials are dominated in EDLCs while conducting polymers and transition metal oxides are commonly used as electrode materials for pseudocapacitors. Due to the low cost, facile synthesis, controllable electrical conductivity, and high pseudocapacitance,[11–13] PAni as a conducting polymer has been considered as one of the most promising pseudocapacitor materials. Unfortunately, PAni suffers from a large volumetric swelling and shrinking during doping/dedoping process as a result of repeated insertion/de-insertion of electrolyte ions.[14–16] The poor mechanical stability often leads to cracks, breaking, and thus fast capacitance decay of PAni-based pseudocapacitors.[1,13] Recently, much effort has conducted in order to stabilize PAni pseudocapcitors by various techniques. Liu et al. prepared carbonaceous coated PAni nanowire by a hydrothermal method, and the pseudocapacitor based on these PAni@C showed a capacitance of 787.40 mF cm^{-2} (189.73 F g^{-1}) with enhanced cycling stability(≈95% retention after 10 000 cycles) in the there-electrode measurement.[17] Wu et al. combined PAni and graphene to generate graphene/PAni nanofiber composites film for supercapacitors with a large electrochemical capacitance (210 F g^{-1}) at a discharge rate of 0.3 A g^{-1} and improved electrochemical stability (≈74% retention after 800 cycles at current density of 3 A g^{-1}).[18] Wang et al. reported a route to grow mesoporous polyaniline film on ultrathin graphene sheets by in situ polymerization using graphene–mesoporous silica composite as template, and the supercapacitor using this composite showed a maximal capacitance of 749 F g^{-1} at 0.5 A g^{-1} in the three-electrode test, as well as achieving capacitance retention of 88% at 5 A g^{-1} after 1000 cycles.[19] Additionally, conducting polymers doped with organic molecules such as *p*-toluenesulfonate have also found to be an alternative method to enhance their cycling stability (≈96% capacitance retention after 500 cycles).[20]

C. Xia, Dr. W. Chen, Dr. X. B. Wang,
Dr. M. N. Hedhili, N. N. Wei, Prof. H. N. Alshareef
Materials Science and Engineering
King Abdullah University of Science
and Technology (KAUST)
Thuwal 23955–6900, Saudi Arabia
E-mail: husam.alshareef@kaust.edu.sa

DOI: 10.1002/aenm.201401805

However, the above-mentioned studies showed relatively low capacitance with limited enhancement of cycling stability for PAni-based pseudocapacitors. It is so far a great challenge to stabilize PAni pseudocapacitors while maintaining their high capacity. Furthermore, the fabrication of two-electrode full cell devices is meaningful for real-life energy storage application.[21]

Herein, we report a novel approach to fabricate nanostructured core–shell PAni–RuO_2 nanofiber arrays for highly stable PAni pseudocapacitors with much improved electrochemical performance. The ultrathin RuO_2 shell achieved by atomic layer deposition (ALD) as a buffer layer not only effectively prevents the damage of the PAni structures during charge and discharge processes, but also facilitates the charge transfer and the electrolyte ion diffusion to the PAni electrodes. The symmetric pseudocapacitors of PAni/RuO_2 core–shell nanofiber arrays show an ultrahigh specific capacitance of 710 F g^{-1} at 5 mV s^{-1} (in full cell configuration), and enhanced cycling stability at very high current density (≈88% capacitance retention after 10 000 cycles at 20 A g^{-1}). This study shows a new strategy toward fabrication of conducting polymers based pseudocapacitors with high stability and good energy storage performance.

2. Results and Discussion

The fabrication of PAni–RuO_2 core–shell nanofiber arrays is shown in **Figure 1**, which involves a dilute chemical polymerization of PAni nanofiber arrays on pristine carbon fiber cloth followed by an ALD growth of ultrathin RuO_2 layer. The as-fabricated PAni–RuO_2 core–shell nanofiber arrays inherit the macroporous nature of the pristine carbon cloth, while possessing the nanoscale characteristics of the PAni–RuO_2 core–shell fibers. Typically, vertically aligned polyaniline arrays (**Figure 2**b) were successfully grown on carbon fiber cloth by dilute chemical polymerization according to the literature,[22] as can be differentiated them from the smooth surface of the pristine carbon cloth fibers (Figure 2a). The as-formed PAni arrays maintain high specific area and ordered nanostructures with thickness of about 300 nm (Figure 2b and Figure S1, Supporting Information). Unfortunately, the pure PAni arrays based pseudocapacitors did not show desirable energy storage capacity with stable electrochemical performance as will be shown in the next section. In order to stabilize the PAni pseudocapacitors, an ultrathin layer of RuO_2 was selectively deposited on the PAni arrays by atomic layer deposition to form PAni–RuO_2 core–shell nanofiber arrays based on the following considerations. It was reported that an outer protection layer is important to stabilize the conducting polymer-based electrodes, and the thickness of the outer layer may generate significant differences in the electrochemical performance of the electrodes.[23–25] We therefore prepared various thicknesses of RuO_2 using different ALD cycles (from 50 cycles to 1500 cycles) to form the PAni–RuO_2 core–shell nanostructures. ALD is an important ultrathin film growth technique with conformal deposition in atomic level control.[26] The ALD method thus enables deposition of uniform and conformal ultrathin films on very high-aspect-ratio substrates[27,28] or nanoparticles.[29] Importantly, ALD at low growth temperature offers good opportunity to retain the basic properties of the polymer matrix. Although ALD and RuO_2 are currently somewhat expensive technique and material, the present study utilized only a very small amount of RuO_2 consisting of only 100 cycles to achieve the optimized performance. Thus, the material cost for the ultrathin RuO_2 layer is relatively low. Moreover, the cost of the PAni–RuO_2 devices can be further decreased when they are scaled up for mass production.

Figure 2c,d show the morphology and microstructure of the PAni–RuO_2 composite with 500 ALD cycles of RuO_2 at different magnifications. The close-up image (Figure 2d) demonstrates that the PAni array still retains its basic morphology even after 500 ALD cycles of RuO_2, thanks to the conformal deposition nature of the ALD process. Moreover, the macroporous nature of the carbon fiber cloth is also maintained (no blocking of its macropores, as shown in the inset of Figure 2c). It is believed that the high specific area and porous structure are favorable

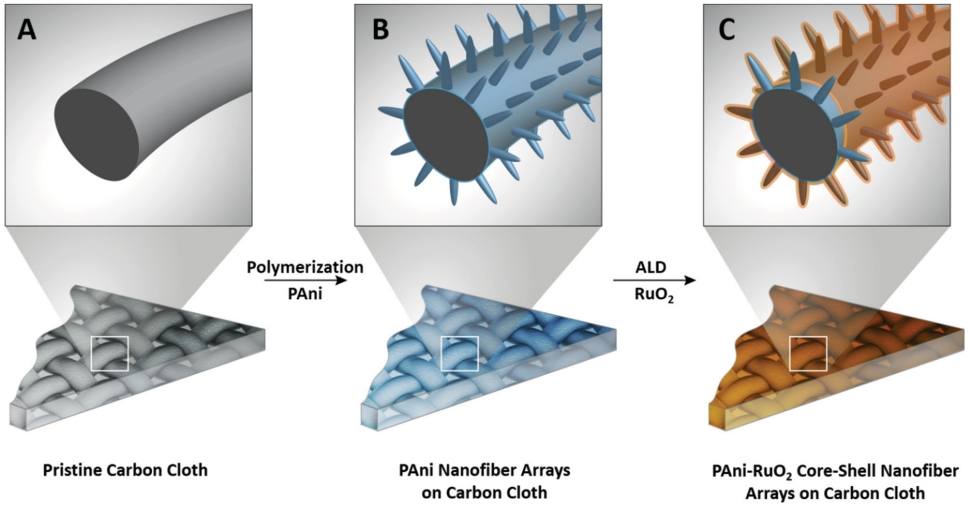

Figure 1. Schematic of the design process of PAni–RuO_2 core–shell nanofiber arrays on carbon cloth as an electrode for symmetric pseudocapacitor. a) Pristine carbon fiber woven cloth; b) PAni nanofiber arrays on carbon cloth by dilute polymerization of aniline; c) PAni–RuO_2 core–shell nanofiber arrays on carbon cloth by further ALD growth of RuO_2 on the PAni nanofiber arrays.

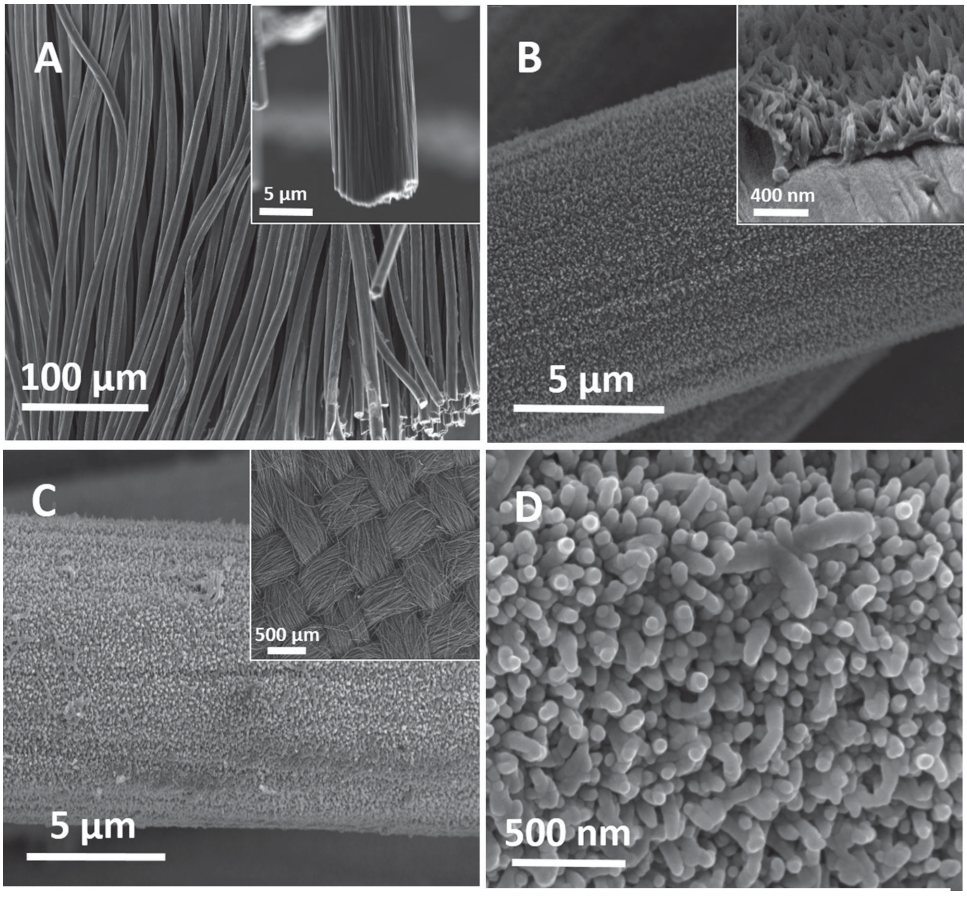

Figure 2. FESEM images of a) pristine carbon fiber cloth; b) PAni nanofiber arrays and; c,d) PAni–RuO_2 core–shell nanofiber arrays with 500 ALD cycles of RuO_2.

for the effective contact between the electrolyte ions and active materials, which leads to enhanced charge storage capacity.

Transmission electron microscopy (TEM) was conducted to further verify the core–shell structure of PAni–RuO_2. As shown in **Figure 3**a–c and Figure S2 (Supporting Information), a uniform shell with thickness of ≈1.7, ≈5.2, and ≈11 nm was observed for samples of 100, 500, and 1500 ALD cycles of RuO_2, respectively. The darker regions at the edge of the core–shell structures are the RuO_2 coating layers. Even after 1500 ALD cycles of RuO_2, the PAni nanofibers appear to be conformally coated with the RuO_2 layer and no clusters are obviously seen. The lattice fringes with different orientations shown in Figure 3d suggest that the deposited RuO_2 is polycrystalline in nature, which is confirmed by its selected area electron diffraction (SAED) pattern. Figure 3e shows the STEM EDS line scans of the core–shell composite for ruthenium and nitrogen. EDS line scanning across the core–shell nanofiber reveals that the profile of Ru has a broad spectrum throughout the entire diameter while the peaks for N are only prominent at the core region, corresponding to the RuO_2 shell and the PAni core, respectively. The analysis of TEM images (Figure 3f) revealed that the variation of the RuO_2 shell thickness is directly proportional to the number of deposition cycles, as expected for ALD deposition process.[23]

The composition of the PAni–RuO_2 core–shell nanofiber was further investigated by SEM energy-dispersive X-ray spectroscopy (EDS) elemental mapping and X-ray photoelectron spectroscopy (XPS). Figure S3 (Supporting Information) reveals that the PAni–RuO_2 nanocomposites possess uniform elements distribution consisting of nitrogen, ruthenium, and oxide. Undoubtedly, this nitrogen comes from the polyaniline nanofiber arrays. From Figure S3c,d (Supporting Information), the even distribution of ruthenium and oxide confirms the successful uniform deposition of RuO_2. XPS analysis was employed to further study the chemical state of element of ruthenium. The survey XPS spectrum of PAni–RuO_2 core–shell nanofibers with 500 ALD cycles of RuO_2 (Figure S4, Supporting Information) shows all the existing elements which match well with EDS measurement. In **Figure 4**a, the doublet peaks at 281 and 285.2 eV originate from RuO_2 due to the screened final state, and the doublet peaks at 282.1 and 286.3 eV are also ascribed to RuO_2 due to the unscreened final-state.[30–32] Another peak at 285.1 eV is associated with C 1*s* peak coming from our carbon fiber support. The XPS peaks of N 1*s* (Figure 4b) are further decomposed into three Gaussian peaks with binding energies of 398.6, 399.7, and 400.6 eV. The peaks locate at 398.6, 399.7, and 400.6 eV are assigned to the quinoid imine (–N=), benzenoid amine (–NH–), and nitrogen cationic ($–N^+–$) of PAni,

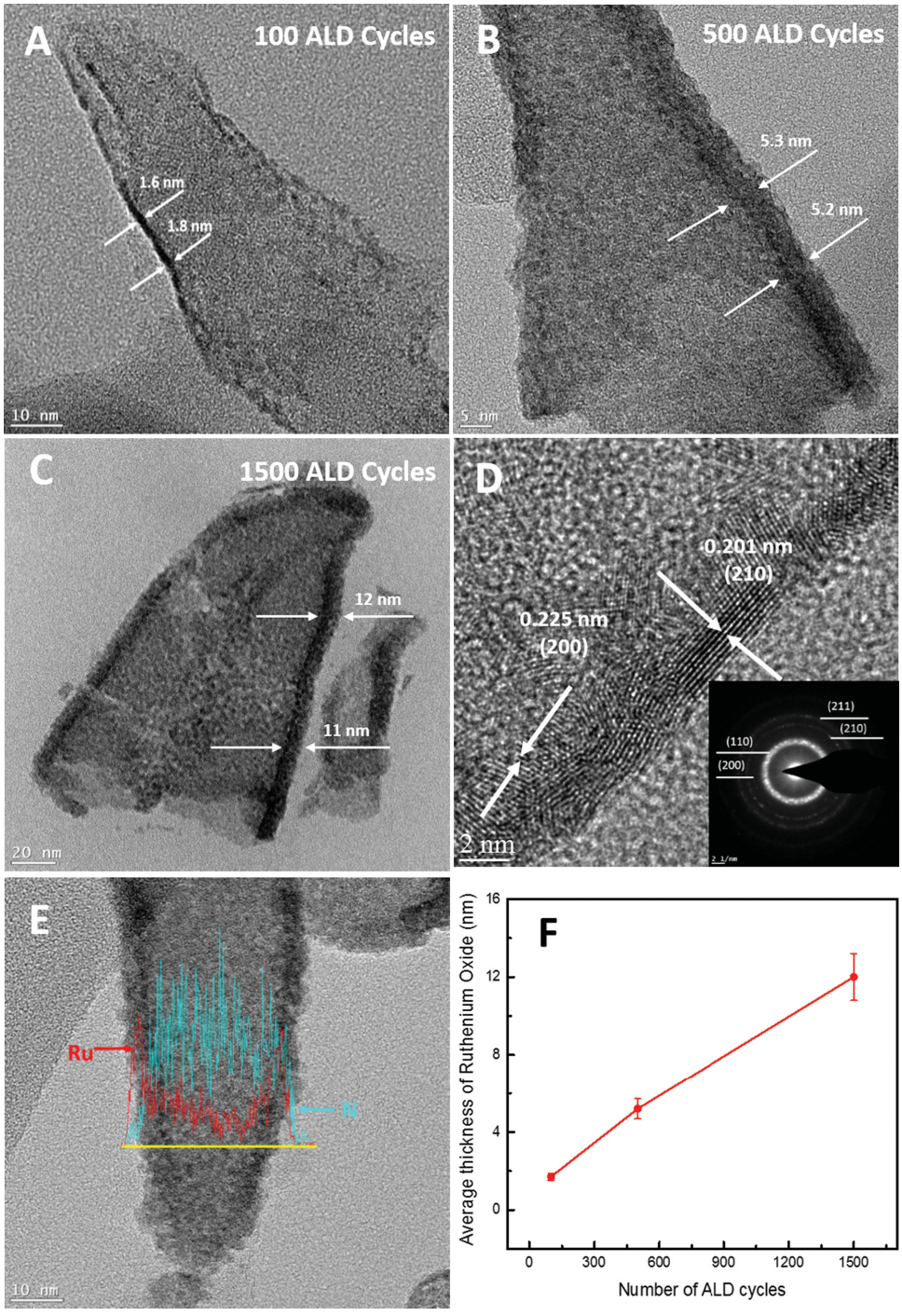

Figure 3. TEM characterization of PAni–RuO_2 core–shell nanofiber with different ALD cycles of RuO_2. a) 100 ALD cycles, b) 500 ALD cycles, c) 1500 ALD cycles; d) HRTEM image and SAED pattern of PAni-500 ALD cycles of RuO_2 sample, e) STEM EDS line scan of PAni-500 ALD cycles of RuO_2 sample, the red and blue lines represent counts of ruthenium and nitrogen signals along the solid yellow line. f) The changes in average thickness of RuO_2 coating with different ALD cycles of RuO_2 on PAni nanofiber arrays.

respectively.[33] The EDS and XPS results further suggest the good integration of RuO_2 shell on PAni nanofiber arrays.

Raman spectra were also carried out to characterize the PAni–RuO_2 core–shell nanofiber with 500 ALD cycles of RuO_2 (Figure S5, Supporting Information). Apart from the D and G bands of carbon fiber cloth, the spectra of neat PAni show characteristic bands at 1162, 1216, 1412, 1486, 1567, and 1615 cm^{-1} corresponding to C–H bending of quinoid ring, C–N stretching of benzenoid ring, C–C stretching of quinoid ring, C=N stretching vibration of quinonoid ring, C=C stretching vibration of quinoid ring, and C–C stretching of the benzenoid ring, respectively.[34,35] The absence of the obvious

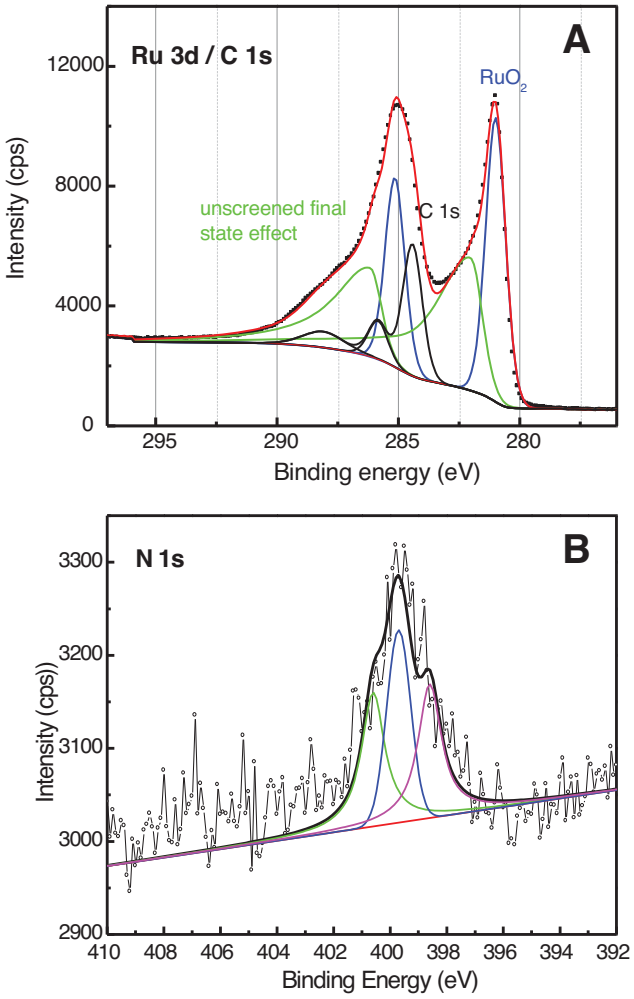

Figure 4. XPS of PAni–RuO_2 core–shell nanofiber with 500 ALD cycles of RuO_2. Core-level spectra of a) Ru 3*d* and C 1s, b) N 1s.

RuO_2 characteristic peaks from Raman spectra is probably due to the ultrathin layer of the RuO_2 on the PAni nanofiber-carbon cloth substrate for enough Raman signals acquisition. Meanwhile, the considerable overlap of Raman peaks of RuO_2 and PAni from 400 to 800 cm^{-1} also made the RuO_2 peaks hard to be distinguished. However, the three major Raman features, namely, the E_g (located at 513 cm^{-1}), A_{1g} (located at 630 cm^{-1}), and B_{2g} (located at 701 cm^{-1}) modes are obviously observed on RuO_2 thin film deposited on glass by 500 ALD cycles, as shown in Figure S6 (Supporting Information).

The electrochemical performances of bare PAni and PAni–RuO_2 core–shell nanofiber arrays were evaluated using two-electrode symmetric pseudocapacitors and investigated in 1 M H_2SO_4 electrolyte solution. **Figure 5**a shows the cyclic voltammetry (CV) of PAni-100 ALD cycles of RuO_2 core–shell nanofiber arrays under different scan rates. The quasi-rectangular CV curves demonstrate a typical pseudocapacitor-like behavior, resulting from both PAni and RuO_2.[36] The pair of redox peaks shown in CV curves is ascribed to the Faradaic transformation of the emeraldine-pernigranilin form of PAni.[13] The anodic peaks shift to higher potential while the cathodic peaks shift to lower potential as the increased scan rate due to the faster charge and discharge rates. This yields wider potential differences between anodic and cathodic peaks, resulting in the capacitances decrease. The galvanostatic charge–discharge (CD) curves (Figure 5b) show symmetric mirror-like feature of charge and discharge process, implying the high efficiency of the pseudocapacitor and highly reversible redox reaction taking place in the PAni–RuO_2 core–shell nanofiber arrays. Even at very high current density (such as 100 A g^{-1}), the voltage (*IR*) drop observed from the CD curve is still very small, which indicates the low value of equivalent series resistance (ESR). These excellent electrochemical features are believed to contribute to high power output for the PAni–RuO_2 core–shell nanofiber pseudocapacitors.

Figure 5c,d summarize the results of CV and CD measurements of bare PAni nanofiber arrays and PAni–RuO_2 core–shell nanofiber pseudocapacitors with different ALD cycles of RuO_2. At the same scan rate of 100 mV s^{-1}, it's obvious that the integrated area of CV curves of different samples (from bare PAni to 1500 ALD cycles of RuO_2) firstly increase from bare PAni to the sample of 100 ALD cycles of RuO_2 on PAni and then decrease dramatically from 100 to 1500 ALD cycles of RuO_2 on PAni, suggesting the change of energy storage capacity by the influence of the ALD cycles of RuO_2 (Figure 5c). The CD curves also illustrate the varied discharge periods with different ALD cycles of RuO_2 on PAni at the constant current density of 20 A g^{-1}, consistent with the electrochemical behavior of the CV curves (Figure 5d). To be specific, the PAni–RuO_2 core–shell nanofibers reach the best electrochemical performance at 100 ALD cycles of RuO_2. Figure 5e presents specific and areal capacitance of all studied samples. It is clear that the specific capacitance of 100 ALD cycles of RuO_2 on PAni has much higher specific capacitance (710 F g^{-1} at 5 mV s^{-1}, corresponds to 354 mF cm^{-2}) than that of bare PAni (564 F g^{-1} at 5 mV s^{-1}, 230 mF cm^{-2}), and 1500 ALD cycles of RuO_2 on PAni (484 F g^{-1} at 5 mV s^{-1}, 196 mF cm^{-2}). Furthermore, the specific capacitance of 710 F g^{-1} at 5 mV s^{-1} obtained by 100 ALD cycles of RuO_2 on PAni-based pseudocapacitor is one of the highest values reported so far for PAni-based full cell devices in aqueous electrolytes under relatively high mass loading of the active materials.[37,38] Notably, at high scan rate of 100 mV s^{-1}, the specific capacitance of PAni-100 ALD cycles of RuO_2 core–shell nanofiber sample can still be up to 667 F g^{-1}, corresponding to a high rate capability of 94%. Even at very high scan rate of 500 mV s^{-1}, this PAni-100 ALD cycles of RuO_2 core–shell nanofiber-based pseudocapacitor still retained 68% of its initial specific capacitance, demonstrating excellent rate performance. The ultrahigh specific capacitance and good rate performance may be related with efficient utilization of the active material as a result of the vertical aligned core–shell structure and the porous feature of the whole electrode design. Additionally, the controllable RuO_2 shell is directly grown on the vertical aligned PAni arrays, resulting in the strong bonding and coupling between PAni and RuO_2 in the hybrid nanostructure, which can significantly enhance the charge transfer of the electrode.[39] Most importantly, the highly conductive vertical aligned PAni–RuO_2 core–shell nanofiber arrays contact directly with the carbon cloths to form an integrated electrode with superb highways for fast electron transportation and electrolyte

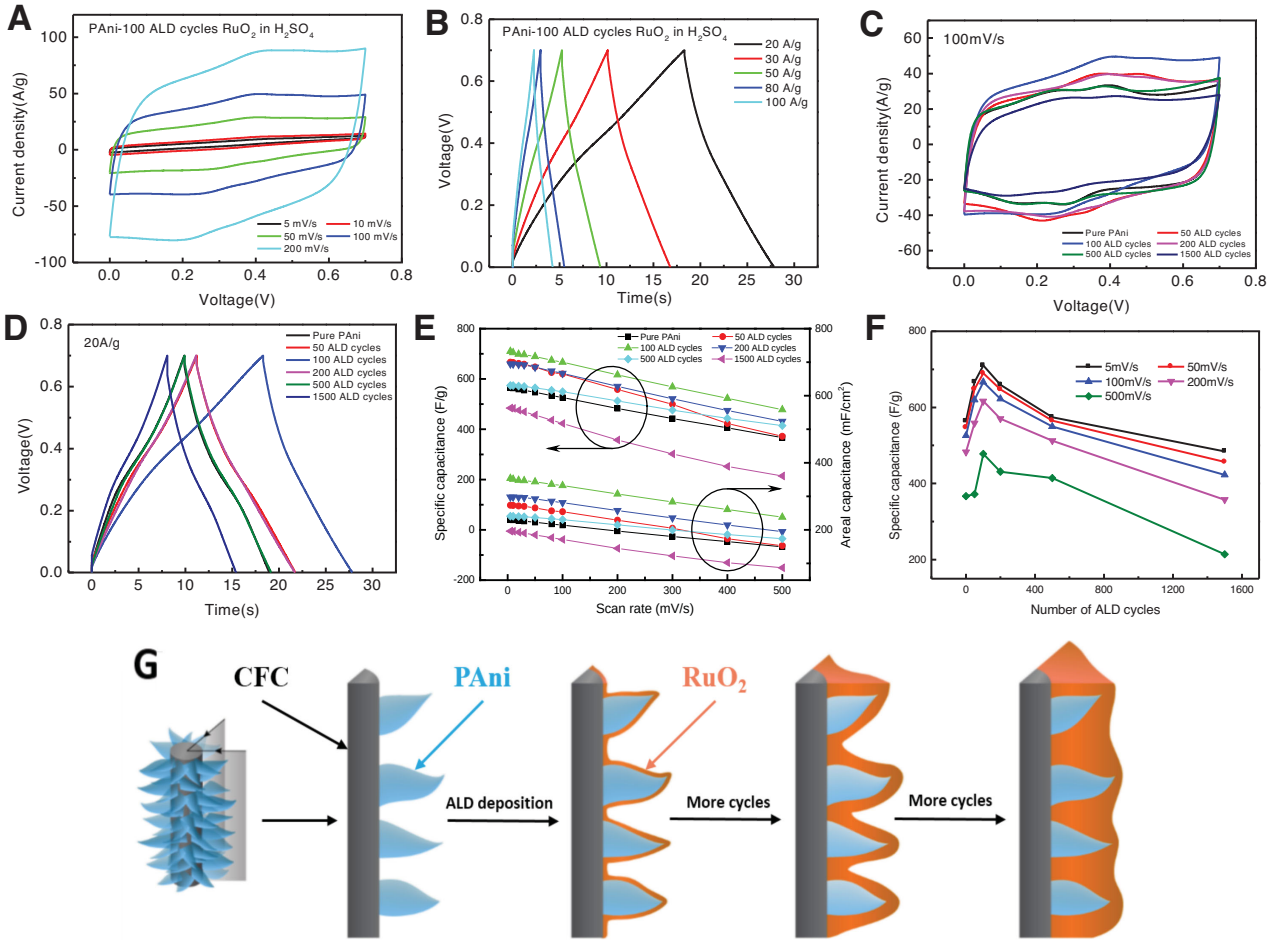

Figure 5. Electrochemical performance of PAni–RuO_2 core–shell nanofiber arrays based symmetric pseudocapacitors. a) Cyclic voltammetry and b) galvanostatic charge–discharge profiles of PAni-100 ALD cycles of RuO_2 based pseudocapacitor; c) cyclic voltammetry, and d) galvanostatic charge–discharge profiles for pseudocapacitors of PAni–RuO_2 core–shell nanofibers with different ALD cycles of RuO_2; e) summary of specific and areal capacitance as function of scan rate; f) summary of specific capacitance as function of ALD cycles; g) schematic of the change of ALD cycles of RuO_2 on PAni nanofiber arrays.

ions diffusion, which greatly increase the charge rate of the device for high-power and energy applications.

Figure 5f shows that the specific capacitance of our pseudocapacitors is strongly correlated to the number of ALD cycles. Among different ALD cycles of RuO_2 for PAni–RuO_2 pseudocapacitors, the PAni-100 ALD cycles of RuO_2 core–shell nanofiber-based pseudocapacitor shows the optimized performance in spite of different scan rates. It reveals that an optimized thickness of RuO_2 layer (≈1.7 nm) is required for PAni pseudocapacitors with high performance. The thickness correlated electrochemical performance of PAni–RuO_2 pseudocapacitors can be explained by the schematic in Figure 5g. Originally, the pure PAni-based pseudocapacitors will undergo significant volume alteration during the cycling tests, leading to the failure of the cells. When a certain thin RuO_2 layer is conformally and homogenously coated on the PAni nanofibers, the PAni electrode can be effectively protected from the mechanical change due to the robust electrochemical stability of the RuO_2 layer. The high conductivity of RuO_2 in the PAni–RuO_2 core–shell nanofiber facilitates the fast electron transportation in the electrode for facile redox reactions of PAni with the electrolyte. Meanwhile, the deposited RuO_2 shell itself is involved in the redox reaction, which synergistically contributes to the higher energy storage capacity of the device. However, too thin layer of the RuO_2 coated PAni showed limited contribution to the improvement of overall device performance, probably due to the limited mechanical constraints of RuO_2 to the fracture of PAni during cycling. Nevertheless, subsequent increase of the RuO_2 thickness is also not desirable for the electrode due to longer diffusion distance of electrons and ions to the PAni core caused by the separation of the thick RuO_2 layer and the limited active redox sites on the surface of RuO_2 layer.[40] Moreover, the dramatic reduction of energy storage capacity of our pseudocapacitor by further increasing the RuO_2 shell thickness will possibly isolate the PAni from the electrolyte during fast charge and discharge process or even block the active reaction sites of the macroporous electrode, resulting in limited redox reactions and hence lower performance devices.[23] The phenomenon of ALD thickness correlated electrochemical performance was also observed in batteries.[41–43] To further understand the unique design and the enhanced electrochemical performance of our PAni–RuO_2 core–shell nanofiber-based pseudocapacitors, we

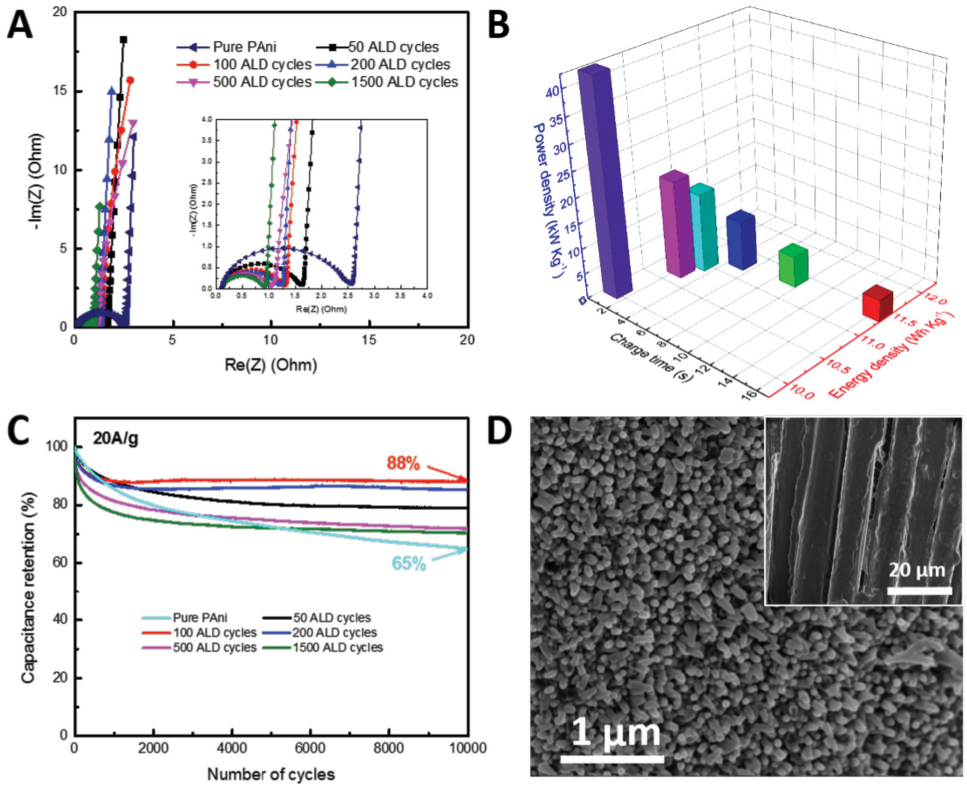

Figure 6. a) Nyquist plots of all PAni–RuO_2 core–shell nanofiber-based pseudocapacitors, b) Ragone plot (energy density vs power density) of PAni-100 ALD cycles of RuO_2 core–shell nanofiber-based pseudocapacitors; c) cycling stability of all PAni–RuO_2 core–shell nanofiber-based pseudocapacitors; and d) FESEM of PAni-100 ALD cycles of RuO_2 core–shell nanofiber electrode and pure PAni electrode (inset) after 10 000 cycles. Note that the PAni structure is completely destroyed without RuO_2 surface coating after 10 000 cycles.

have conducted the measurements of the EDLC contribution and the three-electrode measurements of the PAni and PAni–RuO_2 core–shell electrodes as shown in Figures S7 and S8 (Supporting Information).

The Nyquist plots show the impedance variation of the PAni–RuO_2 core–shell nanofiber-based pseudocapacitors (**Figure 6**a). The nearly vertical line behavior at low frequency for all samples correspond closely to an ideal capacitor.[44] The half circles formed at high frequency range indicate that our pseudocapacitors have very low ESR (≈0.1 Ω), indicating excellent electrical conductivity of the integrated electrodes. The charge-transfer (R_{ct}) resistances are illustrated by the diameters of the half circles shown in Figure 6a (insert). The values of R_{ct} of pure PAni and PAni–RuO_2 core–shell nanofiber-based pseudocapacitors with 50, 100, 200, 500, 1500 ALD cycles are 2.46, 1.53, 1.21, 1.11, 0.95, and 0.81 Ω, respectively. The charge-transfer resistance decreases gradually with the increase of RuO_2 content, which demonstrates the improvements in the conductivity of the electrodes. Figure 6b shows an advanced Ragone plot (energy density vs power density vs charge time) of PAni-100 ALD cycles of RuO_2 core–shell nanofiber pseudocapacitor. The energy and power density were calculated based on cell capacitance, suggesting that the total mass loading of two electrodes is considered. Impressively, the energy density can approach to 10 Wh kg^{-1} at a very high power density of 42.2 kW kg^{-1}, and the corresponding charge time is only ≈1 s. What is more, it is worth noting that with the increase of power density from 4.4 to 42.2 kW kg^{-1}, the energy densities drop very slowly from 11.5 to 10 Wh kg^{-1}. Getting an extremely high power density without large sacrifice of energy density further indicates that the novel nanostructure of PAni–RuO_2 core–shell nanofiber arrays possess significantly enhanced electrochemical performance as pseudocapacitor electrodes. The long-term cycling performance of different PAni–RuO_2 core–shell pseudocapacitors at a very high current density of 20 A g^{-1} for 10 000 cycles are shown in Figure 6c. After 10 000 electrochemical cycles, the PAni-100 ALD cycles of RuO_2 core–shell nanofiber pseudocapacitor still retains ≈88% of its initial capacitance, much higher than that of pure PAni cell (only ≈65% of capacity retention). As a proof-of-concept, the pure PAni and PAni-100 ALD cycles of RuO_2 core–shell nanofiber-based pseudocapacitors after 10 000 cycles were disassembled and investigated by SEM (Figure S9, Supporting Information). Surprisingly, the PAni–RuO_2 core–shell nanofiber-based pseudocapacitor electrode maintained its original morphology very well (Figure 6d), while the PAni nanofibers tend to be fused and merged with each other in the pure PAni pseudocapacitor electrode (inset of Figure 6d and Figure S9, Supporting Information). The better stability of PAni-100 ALD cycles of RuO_2 core–shell nanofiber pseudocapacitor is mainly attributed from the optimized thickness of RuO_2 coating. First, the RuO_2 shell could serve as a mechanical buffering layer that prevents the structural evolution of PAni nanofiber during its charge/discharge cycling. Second, the RuO_2 shell is able to tolerate the volumetric swelling and

shrinking, acting as a conductive network to alleviate the electrode fragments and maintain their mechanical and electrochemical stability.[17] The extraordinary high power density with energy density and good cycling stability make the PAni–RuO_2 core–shell pseudocapacitor as a promising candidate for practical energy storage applications.

3. Conclusion

We have demonstrated for the first time that the deposition of nanoscale RuO_2 shell onto PAni arrays can significantly enhance pseudocapacitive stability and performance. Electrochemical measurements revealed significant enhancement of cycling stability at very high current density, and a high rate capacity using PAni–RuO_2 core–shell structure. The optimized PAni-RuO_2 structure achieved very high specific and areal capacitance (710 F g^{-1} and 354 mF cm^{-2} at 5mV s^{-1}), excellent rate performance (≈94% retention of initial capacitance from 5 to 100 mV s^{-1}), and excellent cycling stability (≈88% retention after 10 000 cycles at 20 A g^{-1}). In addition, our optimized symmetrical pseudocapacitors show very low ESR and rapid charge–discharge characteristic, resulting in exceptionally high power density (42.2 kW kg^{-1} at energy density of 10 Wh kg^{-1}). From the performance we have achieved, we believe that deposition of metal oxide by ALD on conducting polymer is a promising general approach that can be employed to improve the cycling performance of polymer electrodes. Importantly, our results indicate the thickness of metal oxide shell in this heterogeneous nanostructure plays an important role in deciding the electrochemical performance.

4. Experimental Section

Preparation of PAni Nanofiber Arrays: Polyaniline (PAni) arrays were prepared using dilute chemical oxidative polymerization with presence of flexible carbon cloth as described in ref. [22,45]. Typically, 20 mL of 1 M $HClO_4$ aqueous solution was poured into a reaction vessel in an ice bath. A piece of carbon cloth substrate was placed into the vessel. 5 mL of ethanol was added to improve the wettability of the carbon substrate. After the solution was fully cooled, aniline monomer was added into the solution and stirred for 10 min to form a uniform mixture with fixed aniline concentration of 0.01 M. In another beaker, the oxidant, $(NH_4)_2S_2O_8$ (APS), was dissolved in 15 mL 1M $HClO_4$ aqueous solution and precooled (the molar ratio of aniline/APS was 1.5). Next, the oxidant solution was added to the monomer solution, and polymerization was started. The mixture was reacted for 24 h in an ice bath, repeatedly washed with DI water and ethanol, and dried in air after the reaction, thereby yielding the vertical aligned PAni nanofiber arrays on carbon substrate.

Atomic Layer Deposition of RuO_2: Atomic layer deposition of RuO_2 was carried out on Oxford Instrument ALD system FlexAL which provides both thermal and remote plasma-enhanced ALD configurations. A commercially available liquid precursor $Ru(EtCp)_2$ was used as Ru precursor and remote plasma of oxygen as reactant/oxidant respectively. The temperature of precursor was maintained at 75 °C. $Ru(EtCp)_2$ vapor was carried to the process chamber through Ar gas at a flow rate of 150 sccm (standard cubic centimeters per minute).

The ALD process of RuO_2 used follows standard deposition cycle including the following sequence: a pulse of $Ru(EtCp)_2$ vapor, an Ar gas purge, a pulse of oxygen plasma, and another Ar gas purge. In order to achieve the RuO_2 thin film deposition at an acceptable low temperature, modifications to the standard ALD process were implemented. First, an optimization of an early reported modified ALD process was adopted in which a continuous Ar gas diluted oxygen exposure was maintains through all the steps of a standard ALD deposition cycle.[46] The optimized process reduced RuO_2 deposition from a deposition temperature of 265 °C to 170 °C. Second, a $Ru(EtCp)_2$ precursor soaking step inserted between the precursor pulse step and the following Ar gas purge step, with an intention to prolong the dwell time of $Ru(EtCp)_2$. The soaking step reduced the ruthenium precursor usage and helped to achieve a self-limited atomic layer deposition. The RuO_2 deposition temperature was maintained at 180 °C. In order to monitor the deposition process, glass substrate were used together with PAni coated carbon cloth substrate. The following process parameters were employed for the ALD RuO_2 thin film deposition: The ruthenium precursor pulse time is 1.5 s. The following soaking step is 3 s after the precursor valve is closed. The reactant of oxygen plasma step is 4 s and the ALD chamber purge steps are 2.5 s.

Material Characterization: The morphology and microstructure were investigated by SEM (Nova Nano 630, FEI) and TEM (Titan 80–300 kV (ST) TEM, FEI), and the elemental presence and composition were identified using energy-dispersive X-ray spectroscopy (EDS) and XPS analysis (Kratos AXIS Ultra DLD). The Raman spectroscopy was conducted on a Hariba LabRAM HR spectrometer.

Electrochemical Measurements: The electrochemical tests were carried out at room temperature in both three-electrode (half-cell) and two-electrode (full-cell) configurations. In the three-electrode measurements, PAni or PAni-RuO_2 coated carbon cloth was used as the working electrode, a Pt wire as the counter electrode, and saturated calomel electrode (SCE) as the reference electrode. Assembled coin cells for two-electrode configuration were fabricated to sandwich two identical pieces of the electrode samples (≈1 mg of mass loading and ≈1 cm^2 of each electrode) by a monolayer separator (Celgard 3501), and placed inside a coin cell. All electrochemical measurements were carried out at room temperature using VMP3 multichannel electrochemical workstation (Bio-Logic) by the techniques of electrochemical impedance spectroscopy (EIS), cyclic voltammetry (CV), and galvanostatic charge–discharge (CD). The voltage window is from 0 to 0.7 V for both three-electrode measurement and symmetric cell. 1M H_2SO_4 was used as electrolyte for all measurements.

The absolute capacitance (C in F) was obtained from the cyclic voltammograms (CV) or from the CD curves according to the following equations

$$C = \frac{i}{f} \text{ or } C = \frac{I}{\frac{\Delta V}{\Delta t}}$$

where i is average cathodic current of the CV loop and f is the scan rate, and I is the constant current for charge—discharge, and $\frac{\Delta V}{\Delta t}$ is slope of the discharge curve.[47] The specific capacitance and cell capacitance (C_{sp} and C_{cell} in F g^{-1}) were then calculated as

$$C_{sp} = \frac{2C}{m}$$

$$C_{cell} = \frac{C}{2m} \text{ and } C_{areal} = \frac{C}{A}$$

where m is the mass loading of each electrode; and A is the area for each electrode.

The key parameters of the supercapacitor, energy density (E) and power density (P), were calculated based on the total weight of the two electrodes in the full cell devices according to the following equations

$$E = \frac{1}{2} C_{cell} V^2$$

$$P = \frac{E}{\Delta t} = \frac{\frac{1}{2} C_{cell} V^2}{\Delta t}$$

where C_{cell} is the cell capacitance calculated from CD curve, V is the voltage window (0.7 V) applied during the charge–discharge measurement, and Δt is the discharge time obtained from the discharge curve.

Supporting Information

Supporting Information is available from the Wiley Online Library or from the author.

Acknowledgements

C.X. and W.C. contributed equally to this work. Research reported in this publication has been supported by King Abdullah University of Science and Technology (KAUST). Chuan Xia acknowledges supports from the KAUST Graduate Fellowship. C.X. also thanks Dr. Peng Li, Dr. Rakhi, and Dr. Nagaraju at KAUST for several useful discussions. The authors thank the staff of the Nanofabrication Core Laboratory for their excellent support.

Received: October 13, 2014
Revised: November 23, 2014
Published online: January 14, 2015

[1] K. Wang, H. P. Wu, Y. N. Meng, Z. X. Wei, *Small* **2014**, *10*, 14.
[2] M. Armand, J. M. Tarascon, *Nature* **2008**, *451*, 652.
[3] P. Simon, Y. Gogotsi, *Nat. Mater.* **2008**, *7*, 845.
[4] S. Bose, T. Kuila, A. K. Mishra, R. Rajasekar, N. H. Kim, J. H. Lee, *J. Mater. Chem.* **2012**, *22*, 767.
[5] L. L. Zhang, X. S. Zhao, *Chem. Soc. Rev.* **2009**, *38*, 2520.
[6] M. Winter, R. J. Brodd, *Chem. Rev.* **2005**, *105*, 1021.
[7] J. M. Tarascon, M. Armand, *Nature* **2001**, *414*, 359.
[8] A. S. Arico, P. Bruce, B. Scrosati, J. M. Tarascon, W. Van Schalkwijk, *Nat. Mater.* **2005**, *4*, 366.
[9] R. B. Rakhi, W. Chen, D. Cha, H. N. Alshareef, *Adv. Energy. Mater.* **2012**, *2*, 381.
[10] M. Inagaki, H. Konno, O. Tanaike, *J. Power Sources* **2010**, *195*, 7880.
[11] X. Peng, K. F. Huo, J. J. Fu, X. M. Zhang, B. Gao, P. K. Chu, *Chem. Commun.* **2013**, *49*, 10172.
[12] G. P. Wang, L. Zhang, J. J. Zhang, *Chem. Soc. Rev.* **2012**, *41*, 797.
[13] W. Chen, C. Xia, R. B. Rakhi, H. N. Alshareerf, *J. Power Sources* **2014**, *267*, 526.
[14] C. Z. Meng, C. H. Liu, L. Z. Chen, C. H. Hu, S. S. Fan, *Nano Lett* **2010**, *10*, 4025.
[15] T. Kobayashi, H. Yoneyama, H. Tamura, *J. Electroanal. Chem.* **1984**, *177*, 281.
[16] T. Kobayashi, H. Yoneyama, H. Tamura, *J. Electroanal. Chem.* **1984**, *177*, 293.
[17] T. Y. Liu, L. Finn, M. H. Yu, H. Y. Wang, T. Zhai, X. H. Lu, Y. X. Tong, Y. Li, *Nano Lett.* **2014**, *14*, 2522.
[18] Q. Wu, Y. X. Xu, Z. Y. Yao, A. R. Liu, G. Q. Shi, *ACS Nano* **2010**, *4*, 1963.
[19] Q. Wang, J. Yan, Z. J. Fan, T. Wei, M. L. Zhang, X. Y. Jing, *J. Power Sources* **2014**, *247*, 197.
[20] A. Kumar, R. K. Singh, H. K. Singh, P. Srivastava, R. Singh, *J. Power Sources* **2014**, *246*, 800.
[21] M. D. Stoller, R. S. Ruoff, *Energy Environ. Sci.* **2010**, *3*, 1294.
[22] N. R. Chiou, C. M. Lui, J. J. Guan, L. J. Lee, A. J. Epstein, *Nat. Nanotechnol.* **2007**, *2*, 354.
[23] S. Boukhalfa, K. Evanoff, G. Yushin, *Energy Environ. Sci.* **2012**, *5*, 6872.
[24] W. L. Liu, F. C. Lin, Y. C. Yang, C. H. Huang, S. Gwo, M. H. Huang, J. S. Huang, *Nanoscale* **2013**, *5*, 7953.
[25] S. Sim, P. Oh, S. Park, J. Cho, *Adv. Mater.* **2013**, *25*, 4498.
[26] S. M. George, *Chem. Rev.* **2010**, *110*, 111.
[27] J. W. Elam, D. Routkevitch, P. P. Mardilovich, S. M. George, *Chem. Mater.* **2003**, *15*, 3507.
[28] X. Y. Chen, H. L. Zhu, Y. C. Chen, Y. Y. Shang, A. Y. Cao, L. B. Hu, G. W. Rubloff, *ACS Nano* **2012**, *6*, 7948.
[29] J. D. Ferguson, A. W. Weimer, S. M. George, *Thin Solid Films* **2000**, *371*, 95.
[30] W. Wang, S. R. Guo, I. Lee, K. Ahmed, J. B. Zhong, Z. Favors, F. Zaera, M. Ozkan, C. S. Ozkan, *Sci. Rep. -UK* **2014**, *4*, 4452.
[31] M. Zhang, W. Chen, S. J. Ding, Z. Y. Liu, Y. Huang, Z. W. Liao, D. W. Zhang, *J. Phys. D: Appl. Phys.* **2008**, *41*, 3.
[32] D. Rochefort, P. Dabo, D. Guay, P. M. A. Sherwood, *Electrochim. Acta* **2003**, *48*, 4245.
[33] T. Lee, T. Yun, B. Park, B. Sharma, H. K. Song, B. S. Kim, *J. Mater. Chem* **2012**, *22*, 21092.
[34] H. L. Wang, Q. L. Hao, X. J. Yang, L. D. Lu, X. Wang, *Nanoscale* **2010**, *2*, 2164.
[35] T. Lindfors, C. Kvarnstrom, A. Ivaska, *J. Electroanal. Chem.* **2002**, *518*, 131.
[36] J. P. Zheng, P. J. Cygan, T. R. Jow, *J. Electrochem. Soc.* **1995**, *142*, 2699.
[37] Y. Gogotsi, P. Simon, *Science* **2011**, *334*, 917.
[38] G. A. Snook, P. Kao, A. S. Best, *J. Power Sources* **2011**, *196*, 1.
[39] C. L. Long, T. Wei, J. Yan, L. L. Jiang, Z. J. Fan, *ACS Nano* **2013**, *7*, 11325.
[40] X. Sun, M. Xie, J. J. Travis, G. K. Wang, H. T. Sun, J. Lian, S. M. George, *J. Phys. Chem. C* **2013**, *117*, 22497.
[41] Y. C. Perng, J. Cho, S. Y. Sun, D. Membreno, N. Cirigliano, B. Dunn, J. P. Chang, *J. Mater. Chem. A* **2014**, *2*, 9566.
[42] A. Kohandehghan, P. Kalisvaart, K. Cui, M. Kupsta, E. Memarzadeh, D. Mitlin, *J. Mater. Chem. A* **2013**, *1*, 12850.
[43] X. G. Han, Y. Liu, Z. Jia, Y. C. Chen, J. Y. Wan, N. Weadock, K. J. Gaskell, T. Li, L. B. Hu, *Nano Lett.* **2014**, *14*, 139.
[44] M. D. Stoller, S. J. Park, Y. W. Zhu, J. H. An, R. S. Ruoff, *Nano Lett.* **2008**, *8*, 3498.
[45] Y. N. Meng, K. Wang, Y. J. Zhang, Z. X. Wei, *Adv. Mater.* **2013**, *25*, 6985.
[46] J. H. Kim, D. S. Kil, S. J. Yeom, J. S. Roh, N. J. Kwak, J. W. Kim, *Appl. Phys. Lett.* **2007**, *91*, 5.
[47] V. Khomenko, E. Frackowiak, F. Beguin, *Electrochim. Acta* **2005**, *50*, 2499.

